



LAWRENCE  
LIVERMORE  
NATIONAL  
LABORATORY

# Enhanced optical absorption due to symmetry breaking in $\text{TiO}_{2(1-x)}\text{S}_{2x}$ alloys

A. Schleife, P. Rinke, F. Bechstedt, C. G. Van de Walle

October 25, 2012

The Journal of Physical Chemistry C

## **Disclaimer**

---

This document was prepared as an account of work sponsored by an agency of the United States government. Neither the United States government nor Lawrence Livermore National Security, LLC, nor any of their employees makes any warranty, expressed or implied, or assumes any legal liability or responsibility for the accuracy, completeness, or usefulness of any information, apparatus, product, or process disclosed, or represents that its use would not infringe privately owned rights. Reference herein to any specific commercial product, process, or service by trade name, trademark, manufacturer, or otherwise does not necessarily constitute or imply its endorsement, recommendation, or favoring by the United States government or Lawrence Livermore National Security, LLC. The views and opinions of authors expressed herein do not necessarily state or reflect those of the United States government or Lawrence Livermore National Security, LLC, and shall not be used for advertising or product endorsement purposes.

# Enhanced optical absorption due to symmetry breaking in $\text{TiO}_{2(1-x)}\text{S}_{2x}$ alloys

André Schleife,<sup>\*,†,||</sup> Patrick Rinke,<sup>‡,||</sup> Friedhelm Bechstedt,<sup>¶,||</sup> and Chris G. Van de  
Walle<sup>§</sup>

*Condensed Matter and Materials Division, Lawrence Livermore National Laboratory, Livermore,  
California 94550, USA, Fritz-Haber-Institut der Max-Planck-Gesellschaft, Faradayweg 4–6,  
14195 Berlin, Germany, Institut für Festkörpertheorie und -optik, Friedrich-Schiller-Universität,  
Max-Wien-Platz 1, 07743 Jena, Germany, and Materials Department, University of California,  
Santa Barbara, California 93106-5050, USA*

E-mail: a.schleife@llnl.gov

---

\*To whom correspondence should be addressed

†Condensed Matter and Materials Division, Lawrence Livermore National Laboratory, Livermore, California 94550, USA

‡Fritz-Haber-Institut der Max-Planck-Gesellschaft, Faradayweg 4–6, 14195 Berlin, Germany

¶Institut für Festkörpertheorie und -optik, Friedrich-Schiller-Universität, Max-Wien-Platz 1, 07743 Jena, Germany

§Materials Department, University of California, Santa Barbara, California 93106-5050, USA

||European Theoretical Spectroscopy Facility (ETSF)

## Abstract

Titania ( $\text{TiO}_2$ ) is frequently used in photovoltaic and photocatalytic applications, despite the fact that its main optical absorption occurs only at approximately 4 eV. Absorption across the band gap of 3 eV is dipole forbidden in rutile  $\text{TiO}_2$ . By means of first-principles theoretical spectroscopy calculations we demonstrate that alloying with  $\text{TiS}_2$  introduces an absorption band into the fundamental gap of  $\text{TiO}_2$ . In addition, band-edge transitions contribute to optical absorption, because the S incorporation breaks the symmetry of the  $\text{TiO}_2$  lattice. Both effects lead to pronounced absorption of visible light for S concentrations as low as 1.5 %.

## Introduction

Titanium dioxide ( $\text{TiO}_2$ ) has been studied for several decades<sup>1,2</sup> due to its versatility for a diverse range of applications. In the context of photovoltaics or photocatalysis it is used in dye-sensitized solar cells<sup>3</sup> and has great potential for water splitting<sup>4</sup> or the degradation of hazardous substances.<sup>5</sup> Furthermore,  $\text{TiO}_2$  is robust, thermally stable, non-toxic, as well as inexpensive. The large fundamental band gap ( $E_g = 3.03$  eV for the rutile polymorph, see e.g. Refs. 2 and 6) is the reason why  $\text{TiO}_2$  is transparent across the entire visible spectral range. Moreover, direct optical transitions from the valence-band maximum (VBM) to the conduction-band minimum are dipole forbidden, and the main onset of optical absorption occurs only at around 4 eV.<sup>7-11</sup> While this is beneficial for applications as a transparent conducting oxide,<sup>12</sup> it constitutes a problem for the photoactivity since only photons in the ultraviolet range or higher are absorbed.

In order to utilize a larger part of the solar spectrum for photochemical applications, the optical absorption of  $\text{TiO}_2$  has to be extended into the visible part of the spectrum. A number of experimental and theoretical studies have focused on dopants such as N or F<sup>13-16</sup> but also C, Se, P, or S<sup>16-19</sup> as well as co-doping.<sup>19</sup> For S, some of us recently reported that the band gap is drastically reduced as soon as a small amount of S is added to  $\text{TiO}_2$ .<sup>17</sup>

Here we extend this study towards optical properties and show by means of state-of-the-art theoretical spectroscopy techniques that sulfur incorporation not only introduces an alloy band in the

fundamental gap of  $\text{TiO}_2$ , but also breaks the rutile symmetry, which makes direct band-edge transitions dipole allowed. These two factors combined lead to a dramatic increase in absorption in the visible range for S concentrations as low as 1.5 %. Our calculations also explain why experimental studies of S incorporation observed a corresponding red shift of the absorption onset<sup>15,16,20–22</sup> and not the emergence of a defect-related peak in the band-gap region.

## Methodology

We model  $\text{TiO}_{2(1-x)}\text{S}_{2x}$  alloys of different compositions  $x$  ranging from 0 to 0.25 by replacing one O atom with one S atom in rutile supercells of 12 to 96 atoms. The geometries were fully relaxed in density functional theory. Our study focuses on rutile  $\text{TiO}_2$  [space-group:  $P4_2/mnm$  or  $D_{4h}^{14}$  ( $SG136$ )], but the symmetry-breaking mechanism discussed below is expected to also apply to the anatase phase. Optical spectra are calculated using many-body perturbation theory by solving the Bethe-Salpeter equation (BSE).<sup>23</sup>

In a first step, the Kohn-Sham<sup>24</sup> (KS) eigenvalues and eigenstates are calculated using the local-density approximation (LDA)<sup>25,26</sup> to exchange and correlation. The projector-augmented wave method<sup>27</sup> as implemented in the Vienna *Ab-initio* Simulation Package<sup>28,29</sup> is used to describe the electron-ion interaction. Pseudopotentials are the same as used in Ref. 17. From the KS wave functions the optical transition-matrix elements are calculated using the longitudinal approximation.<sup>30</sup>

Excitonic effects as well as local-field effects play a dominant role in the absorption spectra of oxides<sup>31</sup> and their alloys.<sup>32</sup> The description of these effects goes beyond the KS picture and requires the framework of many-body perturbation theory by solving the BSE for the optical polarization function  $P$ .<sup>23</sup> In the optical limit of vanishing photon wave vector the frequency-dependent macroscopic dielectric tensor  $\epsilon_{jj'}(\omega)$  (with  $j, j' = \{x, y, z\}$ ) follows directly from  $P$ .<sup>23</sup> All linear optical properties of a material can then be derived from  $\epsilon_{jj'}(\omega)$ ; specifically, the frequency-

dependent optical absorption coefficient  $\alpha_j(\omega)$ :

$$\alpha_j(\omega) = \frac{\sqrt{2}\omega}{c} \sqrt{|\epsilon_{jj}(\omega)| - \text{Re } \epsilon_{jj}(\omega)} \quad (1)$$

To make the solution of the BSE tractable it is typically rewritten as an eigenvalue problem for the excitonic electron-hole pair Hamiltonian.<sup>23</sup> In our BSE code,<sup>33</sup> the KS eigenstates are used to compute the matrix elements of the statically screened Coulomb attraction between electrons and holes as well as the unscreened exchange terms, both of which determine the excitonic Hamiltonian. In addition, the electron and hole quasiparticle energies are required. While it is desirable to calculate these within many-body perturbation theory in Hedin's *GW* approach,<sup>34</sup> this task is computationally infeasible at the moment, especially for unit cells containing as many as 96 atoms and  $\mathbf{k}$ -point meshes as dense as the ones used in this work (see below). Test  $G_0W_0$  calculations based on LDA input for the 12-atom cell ( $x = 0.25$ ) reveal that the position of the S-induced defect level in the band gap agrees to within 0.05 eV with the scissor-corrected band structure of Ref. 17, in which the occupied bands are rigidly shifted to higher energies. Since the conclusions of the present work are not affected by such a relatively small error, we apply these rigid shifts to all the supercells in this work. The resulting gap of  $\text{TiO}_2$  amounts to 2.98 eV.<sup>17</sup>

Converging the optical absorption spectrum in the vicinity of the band edge requires a large number of  $\mathbf{k}$  points.<sup>35</sup> We use different (hybrid<sup>35</sup>)  $\mathbf{k}$ -point meshes for the different supercells to sample the low-energy transitions, with a maximum  $\mathbf{k}$ -point distance of  $0.36 \text{ \AA}^{-1}$  in all cases. In addition, while the number of conduction bands is increased for the high-energy transitions, the  $\mathbf{k}$  sampling is reduced. A direct diagonalization of the resulting excitonic Hamiltonian matrices quickly becomes infeasible as ranks reach up to 100,000. In this work we therefore employ an efficient time-evolution scheme<sup>36</sup> to calculate  $\epsilon(\omega)$  from the excitonic Hamiltonian. Optical transitions with transition energies larger than the BSE cutoff are included up to 200 eV on the KS level (as described in Ref.<sup>37</sup>) in order to obtain converged results for the real part of  $\epsilon(\omega)$  at low photon energies.

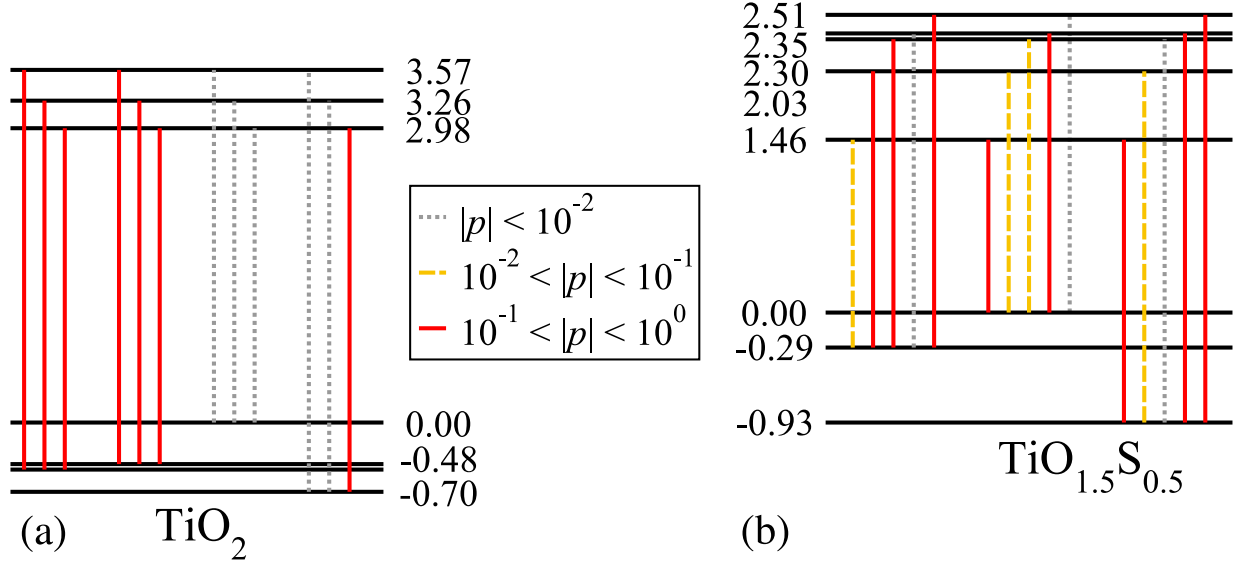


Figure 1: (Color online) Absolute values  $|p|$  (in  $\hbar/a_B$ ) of the optical transition matrix elements for  $\text{TiO}_2$  (a) and the alloy with  $x = 0.25$  (b). The energy zero in both spectra is the VBM. The alloy spectrum has been shifted such that the state that derives from the  $\text{TiO}_2$  VBM is aligned with the VBM in bulk  $\text{TiO}_2$ .

## Results and discussion

We first illustrate the principal effects of S incorporation for the highest concentration. Figure 1 displays the energies of the lowest conduction and highest valence states at the  $\Gamma$  point in  $\text{TiO}_2$  and in the alloy with  $x = 0.25$ , together with the dipole transition matrix elements. The lowest energy transition is dipole forbidden in  $\text{TiO}_2$  independent of the light polarization, and optical transitions across the fundamental gap therefore do not contribute to the onset of absorption. The first transitions with any appreciable weight at the  $\Gamma$  point originate not from the VBM, but from the two bands  $\sim 0.5$  eV lower in energy. These transitions build up to the first strong absorption peak in  $\text{TiO}_2$  at around 4.0 eV.

Replacing one oxygen atom in the rutile unit cell by a sulfur atom introduces S-derived levels in the fundamental gap of  $\text{TiO}_2$ , as seen in Fig. 1(b). The dipole matrix elements for transitions between these states and the  $\text{TiO}_2$ -derived conduction bands are large and contribute considerably to optical absorption in the visible spectral range. However, the S atom also perturbs the rutile crystal structure. A combination of this lattice distortion and the hybridization with S states facilitates

absorption from the states that derive from the band edges in  $\text{TiO}_2$ . This effect adds absorption in the near-ultraviolet spectral region that is absent in pure  $\text{TiO}_2$ , and applies to all S concentrations we have investigated with a strength proportional to the S concentration.

In Fig. 2 we investigate the band structure of  $\text{TiO}_{2(1-x)}\text{S}_{2x}$  with  $x = 0.015625$ , the lowest S concentration we have considered. The alloy exhibits an isolated defect-induced band at  $\sim 0.6$  eV above the bulk VBM of  $\text{TiO}_2$ . This band possesses strong S  $3p$  character, similar to the O  $2p$  symmetry of the VBM. Due to the perturbation by the S atom the gap between the bulk-derived valence- and conduction-band states increases slightly to 3.08 eV.

Figure 2 also depicts the absolute values of the optical transition matrix elements for electronic excitations from the bulk-like valence and the S-induced levels into the conduction bands. In pure  $\text{TiO}_2$  the dipole matrix element vanishes directly at the  $\Gamma$ -point, although the value rises sharply off  $\Gamma$ , as previously observed in  $\text{SnO}_2$ .<sup>31</sup> Sulfur incorporation breaks the rutile crystal symmetry and the transition becomes allowed. Note that even for compositions as low as 1.5 % the perturbation of the lattice symmetry is still strong enough to render transitions from the valence-band edge (that are dipole forbidden in pure  $\text{TiO}_2$ ) as large as the one from the S-induced state.

To support this qualitative discussion, quantitative optical spectra based on the imaginary part of the dielectric function are given in Fig. 3 for different alloy compositions  $x$ . As mentioned above, the first main peak occurs around 4 eV in pure  $\text{TiO}_2$  and originates from lower lying valence bands. Another peak appears around 8.2 eV. The position and the spectral shape of the onset as well as of this second peak agree well with other theoretical results obtained within the Bethe-Salpeter framework.<sup>8-11</sup> Our results also agree with the experimental spectra by Cardona and Harbeke,<sup>7</sup> also included in Fig. 3. The deviation of the energy position of the absorption onset is small; also the curve shape agrees well, in particular for perpendicular light polarization, confirming that our procedure of rigidly shifting unoccupied states is justified.

Increasing the S content in the alloy leads to a considerable reduction of the energy position of the absorption onset. For concentrations as low as 1.5 % the onset has already moved to  $\sim 2.4$  eV, i.e., into the visible spectral range. The absorption below 3 eV can be traced to transitions of

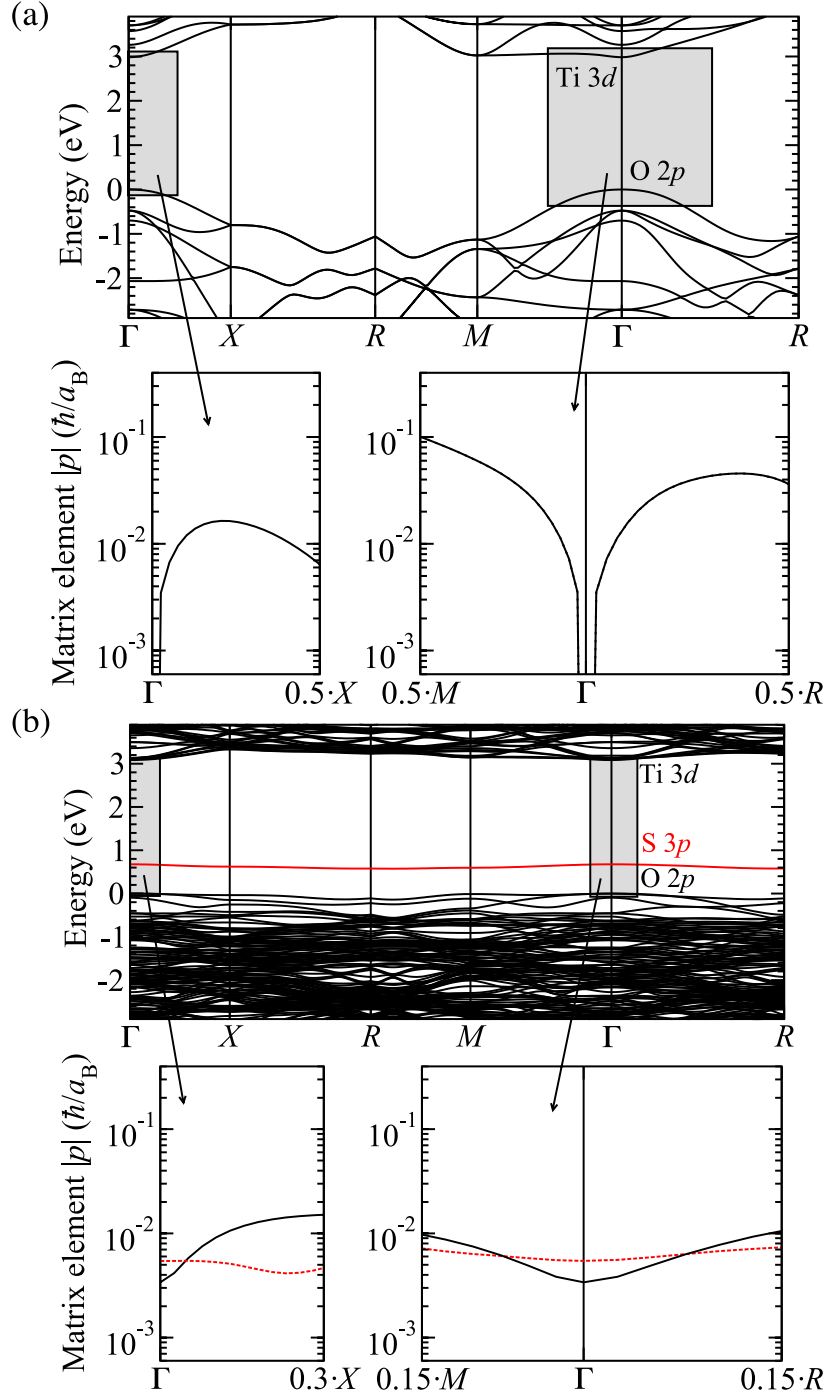


Figure 2: (Color online) Scissor-corrected single-particle band structures of  $\text{TiO}_{2(1-x)}\text{S}_{2x}$  and optical matrix elements for (a)  $x = 0$  and (b)  $x = 0.015625$ . The defect-induced level is shown in red and the VBM of bulk  $\text{TiO}_2$  has been used as energy zero. The optical transition matrix elements  $\frac{1}{2}(|p_x| + |p_y|)$  are plotted for transitions originating from the uppermost bulk-like valence band (black lines) or the defect-induced level (dashed red lines) into the lowest conduction band for the  $\mathbf{k}$ -space regions indicated by the shaded boxes.  $|p_z|$  is too small to be included in the plot.

electrons from the S level into the lowest conduction-band states. However, the small peak around 3 eV for 1.5 % originates from transitions between the bulk-like VBM and the conduction-band minimum that have become dipole allowed. In addition, this peak increases in strength and shifts to smaller energies as the composition  $x$  of the alloy increases; it occurs around 2.5 eV for  $x = 0.25$  (see also Fig. 1).

Increasing  $x$  leads to new peak structures in the imaginary part of the dielectric function especially in the energy range between 2.4 eV and 3.9 eV (see Fig. 3). Spectral weight is shifted from the peak at around 3.9 eV to lower photon energies. This peak, which is very pronounced for pure  $\text{TiO}_2$ , becomes increasingly broad with increasing  $x$ . For  $x = 0.25$  another peak occurs at around 1.5 eV, corresponding to transitions from levels with strong S character.

For a direct comparison to experimentally reported absorption coefficients, we use our calculated dielectric functions to compute  $\alpha(\omega)$  using Eq. (1); the results are shown in Fig. 4. The main effect of S incorporation is to introduce a redshift of the absorption onset, not a defect-related peak in the band gap region; as discussed above, the absorption related directly to the S-induced states is small in magnitude until the S concentration becomes large (approaching  $x = 0.25$ ). The redshift of the absorption onset is considerable even for concentrations as low as 1.5 % and gives rise to notable absorption in the visible spectral region. For larger S concentrations the absorption edge is further red-shifted and the magnitude of absorption in the visible spectral region increases. While this is consistent with experimental observations,<sup>15,16,20–22</sup> our results explicitly show the importance of the symmetry breaking for explaining the observed absorption. This symmetry breaking mechanism should not strongly depend on the nature of the dopant, hence, we expect an impact also for other dopants which is consistent with experimental studies using, for instance, nitrogen.<sup>15,16</sup>

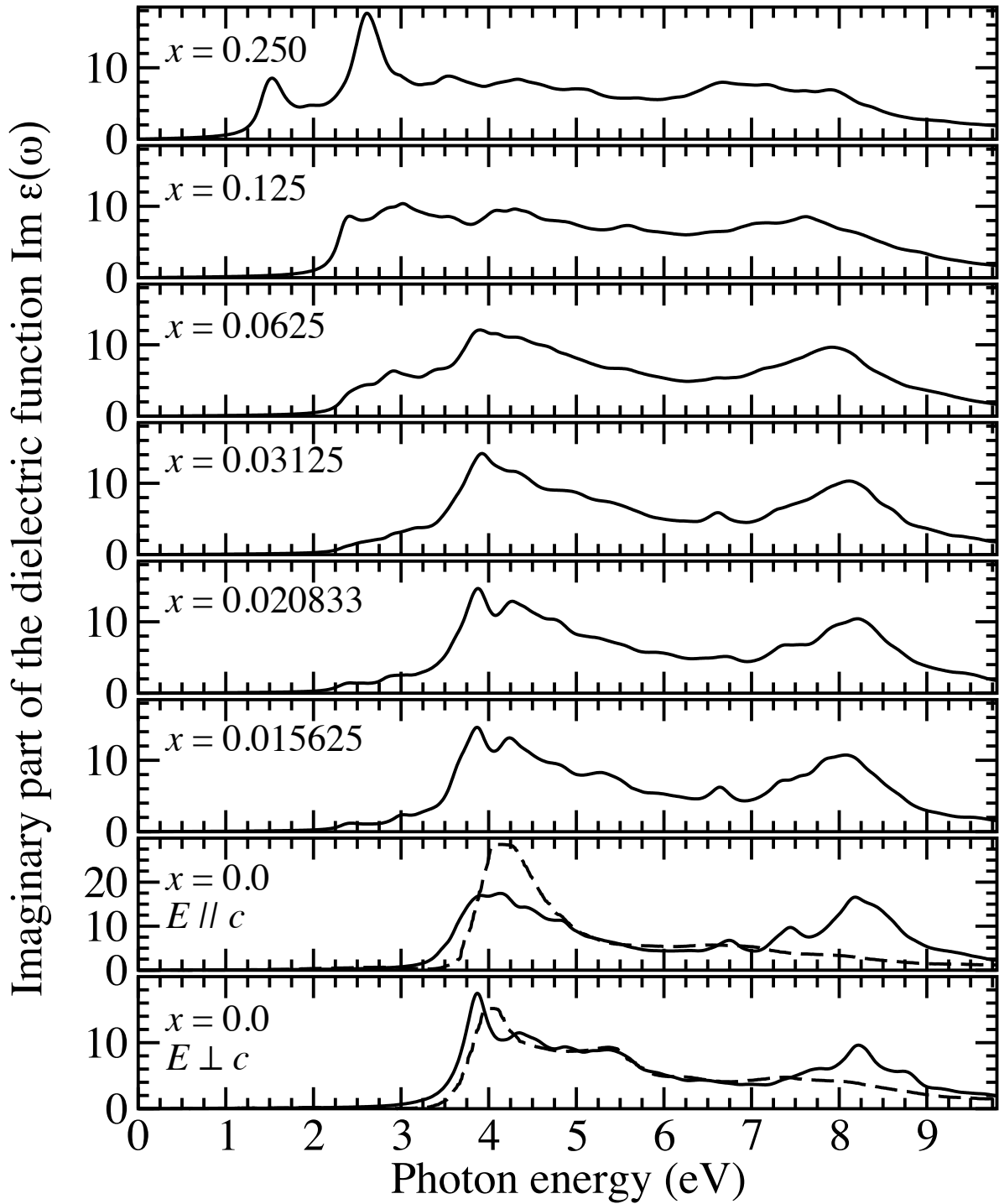


Figure 3: Imaginary part of the dielectric function (averaged over all polarization directions) versus incident photon energy (in eV) for different  $\text{TiO}_{2(1-x)}\text{S}_{2x}$  alloy compositions. A Lorentzian broadening of 0.1 eV is used to account for temperature and lifetime effects. For bulk  $\text{TiO}_2$  we compare the calculated dielectric function to the measurements of Ref. 7 (dashed lines) for two polarization directions.

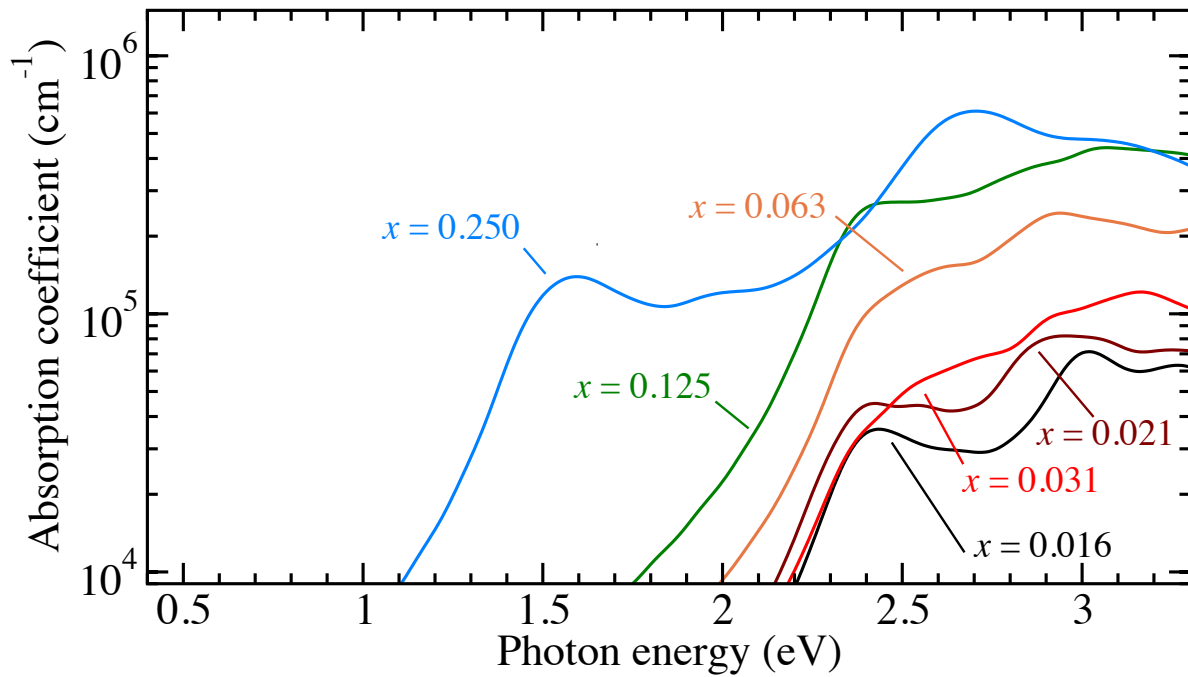


Figure 4: (Color online) Optical absorption coefficient (averaged over all polarization directions) of  $\text{TiO}_{2(1-x)}\text{S}_{2x}$  versus incident photon energy (in eV) for different alloy compositions. A Lorentzian broadening of 0.1 eV is used to simulate temperature and lifetime effects; the resulting sub-band gap absorption in  $\text{TiO}_2$ , which is smaller than  $2 \times 10^4 \text{ cm}^{-1}$  below 2.8 eV, has been subtracted from all the curves.

## Conclusions

In summary, we have presented state-of-the-art theoretical spectroscopy calculations for the optical properties of  $\text{TiO}_{2(1-x)}\text{S}_{2x}$  alloys. S incorporation significantly reduces the energy position of the optical absorption onset compared to pure  $\text{TiO}_2$ . We ascribe this red-shift in part to absorption from a S induced band in the band gap and in part to band-edge absorption that becomes dipole allowed in the alloy due to the broken crystal symmetry. Only at fairly large S concentrations does the absorption from the S-induced band become dominant.

We found the symmetry breaking to be a reason for a significant contribution to optical absorption. Since this mechanism is universal and does not depend on the nature of the dopant, we expect this principle to be transferable to other materials whose band-edge transitions are dipole forbidden such as  $\text{SnO}_2$  or  $\text{In}_2\text{O}_3$ : the incorporation of chalcogenide atoms on the oxygen sublattice should have similar effects as in the case of  $\text{TiO}_2$ .

## Acknowledgement

We acknowledge fruitful discussions with A. Janotti and C. Rödl. AS, PR, and FB gratefully acknowledge financial support by the European Community within the e-I3 project ETSF (GA No. 211956) and the Deutsche Forschungsgemeinschaft (FB: Project No. Be 1346/20-1, PR: Project No. Ri 1507/3-1). CVdW was supported as part of the Center for Energy Efficient Materials, an Energy Frontier Research Center funded by the U.S. DOE, BES under Award Number DE-SC0001009. Part of this work was performed under the auspices of the U.S. Department of Energy at Lawrence Livermore National Laboratory under Contract DE-AC52-07A27344. PR and FB acknowledge the NSF IMI Program (DMR-0843934).

## References

- (1) Grant, F. A. *Rev. Mod. Phys.* **1959**, *31*, 646–674.
- (2) Diebold, U. *Surf. Sci. Rep.* **2003**, *48*, 53–229.

- (3) O'Regan, B.; Grätzel, M. *Nature* **1991**, *353*, 737–740.
- (4) Fujishima, A.; Honda, K. *Nature* **1972**, *238*, 37–38.
- (5) Hoffmann, M. R.; Martin, S. T.; Choi, W.; Bahnemann, D. W. *Chem. Rev.* **1995**, *95*, 69–96.
- (6) Pascual, J.; Camassel, J.; Mathieu, H. *Phys. Rev. B* **1978**, *18*, 5606–5614.
- (7) Cardona, M.; Harbeke, G. *Phys. Rev.* **1965**, *137*, A1467–A1476.
- (8) Kang, W.; Hybertsen, M. S. *Phys. Rev. B* **2010**, *82*, 085203.
- (9) Lawler, H. M.; Rehr, J. J.; Vila, F.; Dalosto, S. D.; Shirley, E. L.; Levine, Z. H. *Phys. Rev. B* **2008**, *78*, 205108.
- (10) Chiodo, L.; García-Lastra, J. M.; Iacomino, A.; Ossicini, S.; Zhao, J.; Petek, H.; Rubio, A. *Phys. Rev. B* **2010**, *82*, 045207.
- (11) Landmann, M.; Rauls, E.; Schmidt, W. G. *J. Phys. Cond. Mat.* **2012**, *24*, 195503.
- (12) Chen, D.; Xu, G.; Miao, L.; hua Chen, L.; Nakao, S.; Jin, P. *J. Appl. Phys.* **2010**, *107*, 063707.
- (13) Umebayashi, T.; Yamaki, T.; Itoh, H.; Asai, K. *Appl. Phys. Lett.* **2002**, *81*, 454–456.
- (14) Varley, J. B.; Janotti, A.; Van de Walle, C. G. *Adv. Mater.* **2011**, *23*, 2343–2347.
- (15) Li, H.; Li, J.; Huo, Y. *J. Phys. Chem. B* **2006**, *110*, 1559–1565.
- (16) Sakai, Y. W.; Obata, K.; Hashimoto, K.; Irie, H. *Vacuum* **2008**, *83*, 683–687.
- (17) Umezawa, N.; Janotti, A.; Rinke, P.; Chikyow, T.; Van de Walle, C. G. *Appl. Phys. Lett.* **2008**, *92*, 041104.
- (18) Long, R.; English, N. J. *J. Phys. Chem. C* **2009**, *113*, 8373–8377.
- (19) Wang, P.; Liu, Z.; Lin, F.; Zhou, G.; Wu, J.; Duan, W.; Gu, B.-L.; Zhang, S. B. *Phys. Rev. B* **2010**, *82*, 193103.

- (20) Ho, W.; Yu, J. C.; Lee, S. *J. Solid State Chem.* **2006**, *179*, 1171–1176.
- (21) Li, H.; Zhang, X.; Huo, Y.; Zhu, J. *Environ. Sci. Technol.* **2007**, *41*, 4410–4414.
- (22) Rockafellow, E. M.; Stewart, L. K.; Jenks, W. S. *Appl. Catal. B-Environ.* **2009**, *91*, 554–562.
- (23) Onida, G.; Reining, L.; Rubio, A. *Rev. Mod. Phys.* **2002**, *74*, 601–659.
- (24) Kohn, W.; Sham, L. J. *Phys. Rev.* **1965**, *140*, A1133–A1138.
- (25) Ceperley, D. M.; Alder, B. J. *Phys. Rev. Lett.* **1980**, *45*, 566–569.
- (26) Perdew, J. P.; Zunger, A. *Phys. Rev. B* **1981**, *23*, 5048–5079.
- (27) Kresse, G.; Joubert, D. *Phys. Rev. B* **1999**, *59*, 1758–1775.
- (28) Kresse, G.; Furthmüller, J. *Phys. Rev. B* **1996**, *54*, 11169–11186.
- (29) Kresse, G.; Furthmüller, J. *Comp. Mater. Sci.* **1996**, *6*, 15–50.
- (30) Gajdoš, M.; Hummer, K.; Kresse, G.; Furthmüller, J.; Bechstedt, F. *Phys. Rev. B* **2006**, *73*, 045112.
- (31) Schleife, A.; Varley, J. B.; Fuchs, F.; Rödl, C.; Bechstedt, F.; Rinke, P.; Janotti, A.; Van de Walle, C. G. *Phys. Rev. B* **2011**, *83*, 035116.
- (32) Schleife, A.; Rödl, C.; Furthmüller, J.; Bechstedt, F. *New J. Phys.* **2011**, *13*, 085012.
- (33) Rödl, C.; Fuchs, F.; Furthmüller, J.; Bechstedt, F. *Phys. Rev. B* **2008**, *77*, 184408.
- (34) Hedin, L. *Phys. Rev.* **1965**, *139*, A796–A823.
- (35) Fuchs, F.; Rödl, C.; Schleife, A.; Bechstedt, F. *Phys. Rev. B* **2008**, *78*, 085103.
- (36) Schmidt, W. G.; Glutsch, S.; Hahn, P. H.; Bechstedt, F. *Phys. Rev. B* **2003**, *67*, 085307.

- (37) (a) Schleife, A. Exciting Imperfection: Real-structure effects in magnesium-, cadmium-, and zinc-oxide. PhD thesis, Friedrich-Schiller-Universität, Jena, 2010; (b) Schleife, A. *Electronic and optical properties of MgO, ZnO, and CdO*; Südwestdeutscher Verlag für Hochschulschriften, 2011.